ELSEVIER

Journal of Materials Processing Technology 192–193 (2007) 340–345

Journal of Materials Processing Technology

www.elsevier.com/locate/jmatprotec

Hybrid laser micro/nanofabrication of phase change materials with combination of chemical processing

Y. Lin [a,b,c], M.H. Hong [b,c,*], G.X. Chen [a], C.S. Lim [a,d], L.S. Tan [c], Z.B. Wang [b], L.P. Shi [b], T.C. Chong [b,c]

[a] *Nanoscience & Nanotechnology Initiative, National University of Singapore, 2 Engineering Drive 3, Singapore 117576, Singapore*
[b] *Data Storage Institute, Agency for Science, Technology and Research, DSI Building, 5 Engineering Drive 1, Singapore 117608, Singapore*
[c] *Department of Electrical and Computer Engineering, National University of Singapore, 4 Engineering Drive 3, Singapore 117576, Singapore*
[d] *Department of Mechanical Engineering, National University of Singapore, 2 Engineering Drive 3, Singapore 117576, Singapore*

Abstract

Phase change materials have been widely applied in optical data storage technique to produce rewritable versions of compact disks and digital versatile disks random access memory and are still promising for higher capacity optical data storage. In optical data storage system, laser irradiation is used to write and read information in phase change film. The original phase state of phase change film without annealing is amorphous state. After laser irradiation, the laser energy transferred to phase change film increases temperature to create crystalline features. To study the effects of laser wavelength and fluence on feature fabrication, different kinds of laser systems are used to irradiate non-annealing phase change film to fabricate crystalline features in micro/nano-sizes. Electrical force microscopy and near-field scanning optical microscopy are used to characterize the electrical and optical properties of phase change film, respectively. Two kinds of phase change film, $Ge_1Sb_2Te_4$ and Sb_2Te_3, are used. Alkaline solution has the ability to etch the amorphous and crystalline states of phase change film selectively. The phase change film patterned by laser irradiation is etched by alkaline solution to fabricate two- and three-dimensional structures. The etching selectivity and rate of alkaline solution for the two phase change films are studied. It provides a novel approach to fabricate new functional micro/nano devices by combining further etching or deposition techniques.

Keywords: Phase change material; Electrical force microscopy; Near-field scanning optical microscopy; Alkaline solution etching

1. Introduction

A high-throughput and low-cost nano-patterning which allows complete freedom in fabricating nano-patterns is still the target of nanolithography techniques. Electron-beam nanolithography, ion-beam nanolithography, X-ray nanolithography, and near-field scanning probe nanolithography have been developed for decades [1–6], whereas they are facing the challenge of low throughput and high cost. Nanoimprint lithography has attracted significant attention recently for its high throughput [7], but it is easy to contaminate expensive stamps for its contact patterning method, which increases processing cost. In this paper, one novel parallel phase change nanolithography technique by laser irradiation through a microlens array (MLA) is developed. MLA has been demonstrated to pattern micro-/nano-structures in polymer uniformly over a large area at a short time [8,9].

The microlenses (same size and focal length in micron-order) in MLA convert a laser beam into thousands of focal points, which act as an array light "pen" to fabricate different tiny structures uniformly over a large area at a high speed. This is a non-contact parallel nanopatterning process in far field. Phase change film is selected as patterned samples. Phase change alloys have two phase states of amorphous and crystalline states, which can transform to each other by the heat treatment. The different optical and electrical properties of these two states of phase change media make it not only widely used in optical data storage, but also as a prime candidate for a random access memory (RAM), which serves as a future alternative to a conventional CMOS based memories.

2. Experimental

Fig. 1 shows the optical image of a MLA and the schematic diagram of the experimental setup. The number of lenses, which are made of fused silica, is

* Corresponding author at: Data Storage Institute, Agency for Science, Technology and Research, DSI Building, 5 Engineering Drive 1, Singapore 117608, Singapore. Tel.: +65 68748707; fax: +65 67771349.
E-mail address: Hong_Minghui@dsi.a-star.edu.sg (M.H. Hong).

0924-0136/$ – see front matter © 2007 Elsevier B.V. All rights reserved.
doi:10.1016/j.jmatprotec.2007.04.089

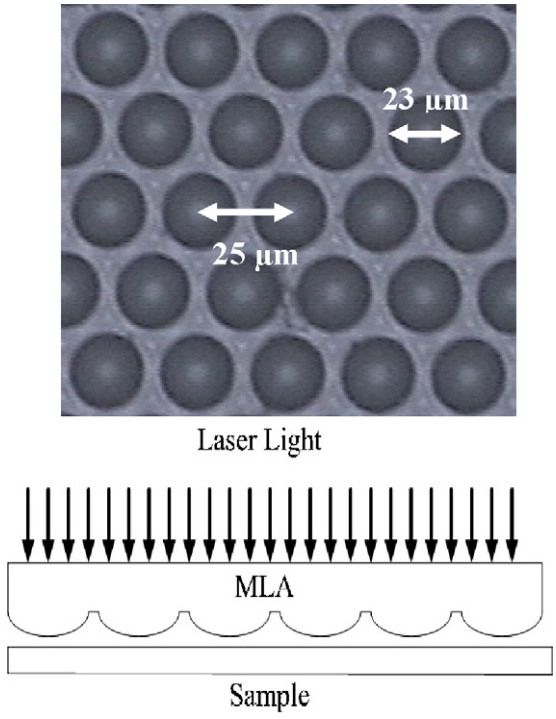

Fig. 1. Optical image of a microlens array (MLA) and schematic diagram of the experimental setup.

401 × 401 in an area of 10 mm × 10 mm. The diameter of the lenses is 23 μm and the lenses are arranged in a hexagonal array with a pitch of 25 μm. The sag of each lens is 9 μm in height, which is equivalent to a focal length of 28.7 μm, thus giving a numerical aperture (NA) of 0.59. $Ge_1Sb_2Te_4$ and Sb_2Te_3 films sputtered on a polycarbonate substrate, and its original state is in the amorphous phase. Different Nd:YAG laser systems: BMI 5000 (pulse repetition rate 10 Hz, pulse duration 7 ns) with fundamental and second harmonic generation at wavelengths of 1064 nm and 532 nm, respectively; Lightwave laser (Series 210G, wavelength 532 nm, pulse repetition rate 1 kHz, pulse duration 40 ns); AVIA laser (wavelength 355 nm, pulse repetition rate 1 kHz, pulse duration 100 ns), and femtosecond (fs) laser (Spectra-physics, wavelength of 800 nm, pulse duration of 100 fs, pulse repetition rate of 80 MHz, and linearly polarized), are used to irradiate the samples through the MLA at different laser fluences. The features on the phase change film are characterized by electrical force microscopy (EFM, DI 3100, Veeco) and near-field scanning optical microscopy (NSOM, Aurora-2, Veeco) in the transmission mode.

3. Results and discussion

3.1. Talbot effect

Fig. 2 shows the optical microscopy images of a series of dot features fabricated in the $Ge_1Sb_2Te_4$ film by Nd:YAG laser irradiation at a fluence of 39.4 mJ/cm^2 with the samples being placed at different distances from the MLA. The crystalline features display a higher reflectivity than the amorphous surroundings. Since the separate distance between the MLA and the GST films are only about tens of microns, it is difficult to measure the exact distance, only the qualitative relationship between distance and feature arrangement was considered in this paper. When the film was placed at the focal plane, the dot features were patterned by the foci of the lenses directly and the feature size was around 1 μm, as shown in Fig. 2(a). When the sample was moved away from the focal plane, the multiple foci resulted in extra dot features as well as different dot feature sizes, as shown in Fig. 2(b–d). The largest dot features were created by the foci of the microlenses, while the smaller features were produced by the multi-sub-foci of foci of MLA, which is due to interference at fractional Talbot planes. Due to the theory of Talbot effect [10–12], the foci number remains same at half of or one Talbot length, and the shorter MLA-to-sample distance inside half of Talbot length leads to greater interference and more multiple foci, so the features shown in Fig. 2(b) were obtained at the nearest distance to the focal plane, while those in Fig. 2(d) were the furthest.

Table 1
Calculated minimum focal spot sizes and smallest feature sizes fabricated by Nd:YAG lasers with different wavelengths at 1064 nm, 532 nm, and 355 nm

	Laser model		
	BMI	Lightwave	AVIA
Wavelength (nm)	1064	532	355
Minimum focal spot size calculated (nm)	1690	845	564
Smallest feature size obtained in experiments (nm)	512	360	220
Experimental/calculated (%)	30	42	39

Talbot effect not only induces multi-sub-foci, but also changes the dot feature structure. Fig. 3 displays the dot features on $Ge_1Sb_2Te_4$ film obtained by fs laser irradiation at a power of 140 mW with 100 pulses at different distances to MLA. The arrangement of dot features was same to MLA. It suggests that these dot features were produced by foci of MLA. The rings appearing around the dots mean that the samples were not placed at the exact focal plane, it may be at half of or integer times of Talbot length. At these distances, no multi-sub-foci appeared, diffraction phenomenon of etch microlens strengthened.

3.2. Laser fluence effect

When the radius of lens is much larger than the wavelength used, the minimum focus spot size of the microlens depends on the laser wavelength described as Eq. (1), where M^2 denotes the laser beam profile quality, λ the wavelength, f the focus length, and d_0 is the size of the lens. The laser beam was approximated as a Gaussian profile, so M^2 is equal to 1. When the lens parameters are fixed, the minimum focal spot size increases with the wavelength linearly:

$$d_{\min} = \frac{4M^2\lambda f}{\pi d_0} \quad (1)$$

Fig. 4 is the dependence of the crystalline feature size in $Ge_1Sb_2Te_4$ film on the incident laser fluence of second harmonic generation of BMI Nd:YAG laser (wavelength 532 nm). The smallest size was around 350 nm. It shows that the feature size increases with laser fluence linearly, which was also observed when using other Nd:YAG lasers, such as BMI laser with 1064 nm, Lightwave laser with 532 nm, and AVIA laser with 355 nm.

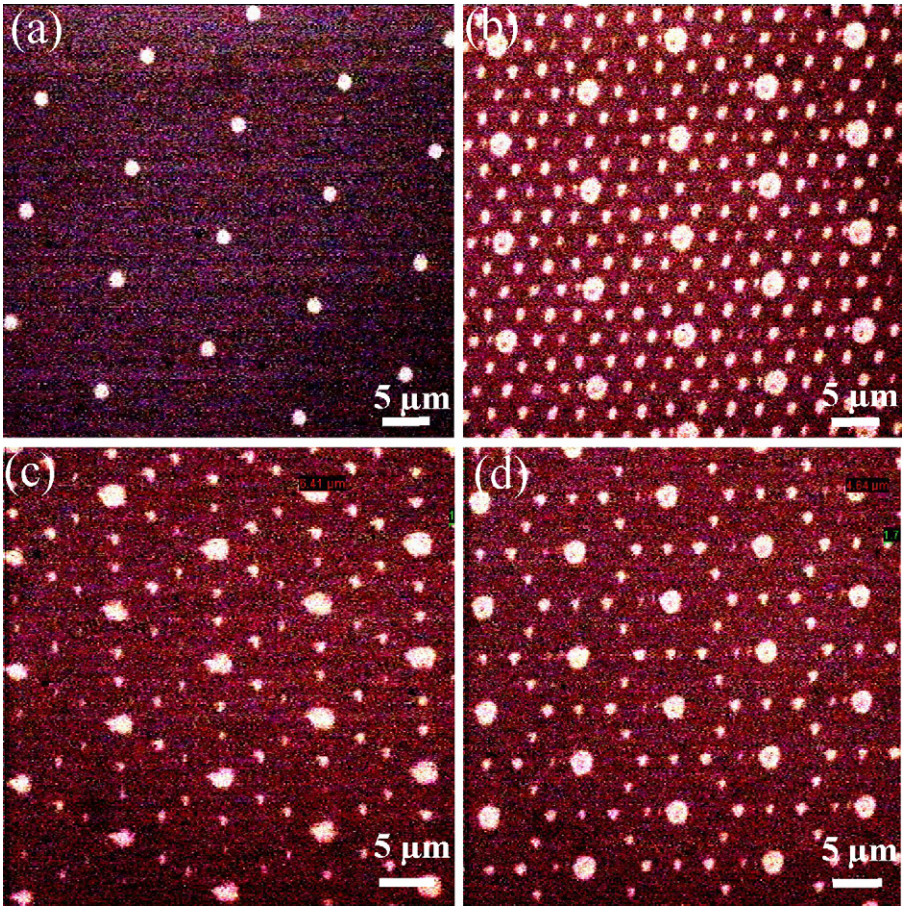

Fig. 2. A series of optical micropatterns produced on the $Ge_1Sb_2Te_4$ film by the laser irradiation of BMI 5000 with wavelength 532 nm through the MLA at a laser fluence of 39.4 mJ/cm^2 but different separate distances between the MLA and phase change film.

Table 1 displays the calculated minimum focal spot sizes and smallest feature sizes fabricated by Nd:YAG lasers with different wavelength at 1064 nm, 532 nm, and 355 nm. It appears that the feature sizes obtained increase with the wavelength used, which is same to the dependence of focal spot size on wavelength. But the smallest feature sizes fabricated are much smaller than the calculated focal spot size. For 1064 nm wavelength, the experimental feature size is only around a third of calculated focal spot size, which is the one reduces mostly in three wavelengths. For 532 nm and 355 nm wavelengths, the percentages are around 40%. This comparison suggests that the feature size is not limited by the minimum focal spot size but will be much smaller. The reason maybe relate to the mechanism of phase state conversion of phase change film. It is using heat treatment to convert the amorphous state to crystalline one by laser irradiation. The laser beam can be assumed as Gaussian beam. When the incident laser fluence is low, only the peak power of the laser pulse is able to heat the film to phase change temperature, which makes the affected area smaller than the focal spot size of the lens.

The feature sizes obtained by the Nd:YAG lasers increased with the laser wavelength used. However, it is completely different for a fs laser. Fs laser with 800 nm was used to irradiate the phase change film. Fig. 5 shows the dependence of crystalline feature sizes in $Ge_1Sb_2Te_4$ film on the pulse number during 800 nm fs laser irradiation. The feature sizes increased with pulse number, but the trend was not linear, which is different to the dependence observed using other laser system. Different to conventional laser, fs laser has an extremely high intensity with very short pulses, which leads to non-linear effects. Many interesting non-linear phenomena have been observed within the fs laser pulses, such as supercontinuum radiation [13], third-harmonic generation [14–16], and electrical conductivity of plasma channels [17,18]. It is believed that this non-linear property of femtosecond laser pulses makes the increase of feature size non-linearly. Making use of fs laser, tiny structures can be fabricated in photoresist [19]. In phase change film, FWHM down to around 50 nm has been achieved [20].

3.3. Phase change film characterization

Electrical force microscopy (EFM) and near-field scanning optical microscopy (NSOM) in the transmission mode were used to characterize the electrical and optical properties of phase change film, respectively. The amorphous phase has a much higher resistivity than crystalline for the lower carrier mobility and smaller carrier concentration in the amorphous phase [21]. On the other hand, reflectivity of crystalline state is higher, which can be observed from the optical image shown in Figs. 2 and 3, while the transmissivity is lower than the amorphous state [22]. Fig. 6 shows the EFM images of two dot features in Fig. 3(a and

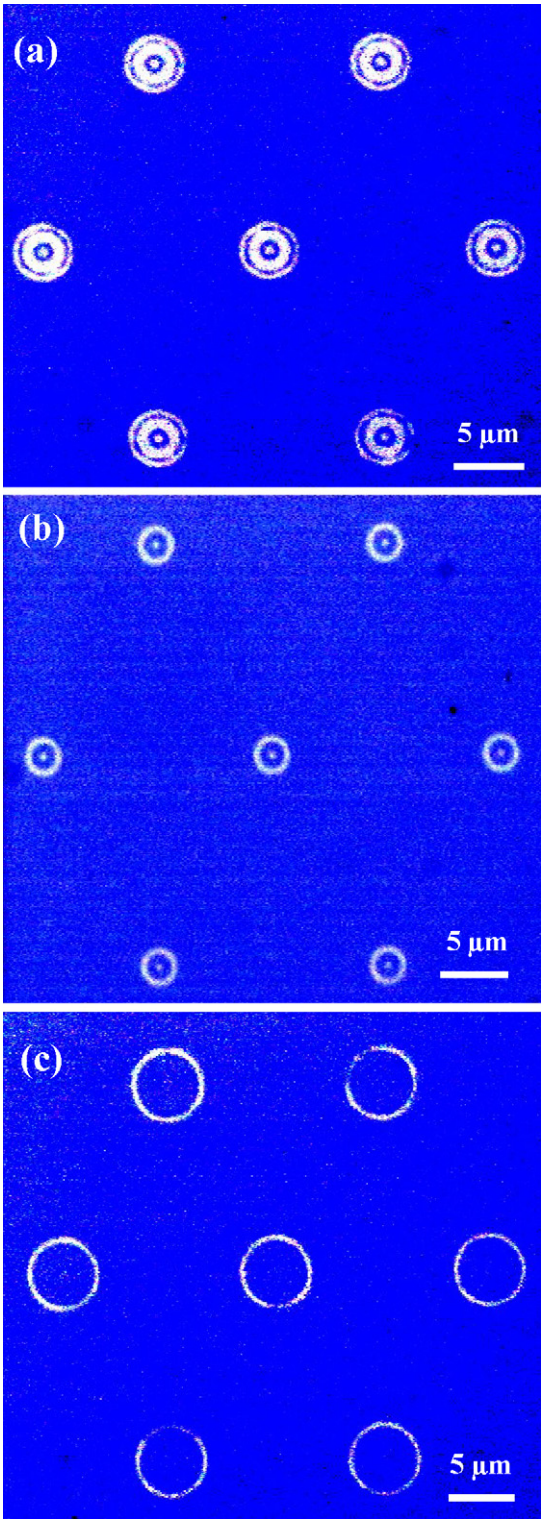

Fig. 3. Optical images of dot features on $Ge_1Sb_2Te_4$ film fabricated by fs laser at a power of 140 mW with 100 pulses at different distances to MLA.

b). The EFM mode used is phase mode. The "phase" signal in EFM is the cantilever amplitude signal, which is proportional to the electrical force and resistivity as well. The applying voltage on the phase change film was 5 V, which was multiplied by the "phase" difference to estimate the resistivity difference between

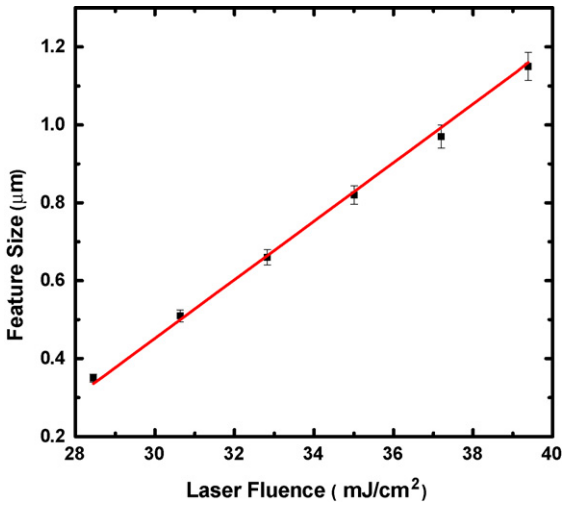

Fig. 4. Dependence of feature size on incident laser fluence with 532 nm of Nd:YAG laser irradiation.

amorphous and crystalline phase states. Since the "phase" difference between the crystalline and amorphous phases was around 0.4° (analyzed from line profile, not shown here), the resistivity of amorphous was around two times over the crystalline features.

Fig. 7 shows 3D transmission NSOM image of crystalline features in the GST film fabricated by the fs laser irradiation through the MLA with a laser power of 200 mW for 100 ms, and the average dot feature size was around 1 μm. It appeared that the crystalline features have lower light transmitivity for its lower PMT output (in voltage unit, dark color). Calculated from the ratio of the highest and lowest PMT output, the transmitivity of crystalline is around 40% of amorphous phase in the film.

3.4. Chemical etching of phase change film

It was found that the phase change film has different reactivity to alkaline solutions at different components. Fig. 8 was AFM images of $Ge_1Sb_2Te_4$ and Sb_2Te_3 films etched by 30% NaOH

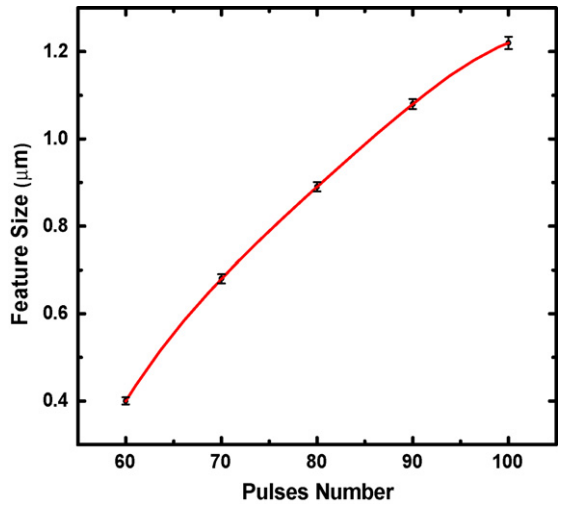

Fig. 5. Dependence of feature size on pulse number during 800 nm fs laser irradiation.

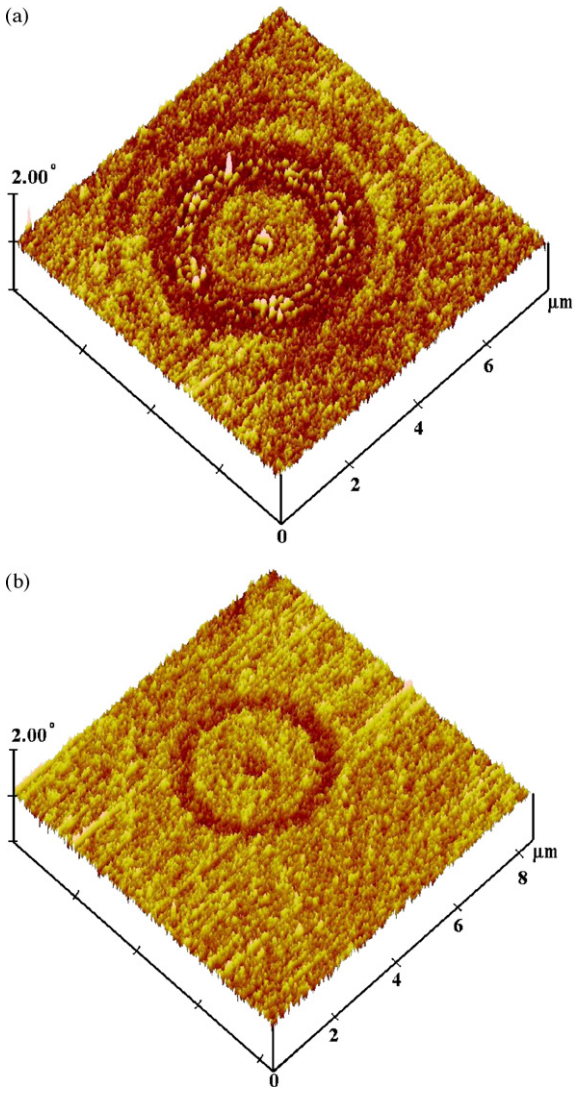

Fig. 6. 3D EFM images of one dot features in Fig. 3(a) and (b).

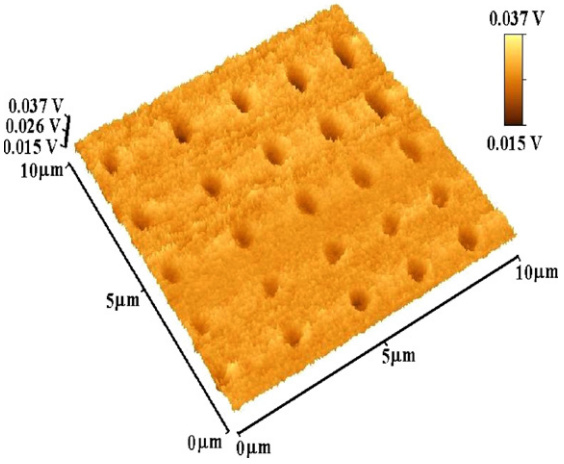

Fig. 7. 3D transmission NSOM image of features in the GST film fabricated by the fs laser irradiation through the MLA with a laser power of 200 mW for 100 ms.

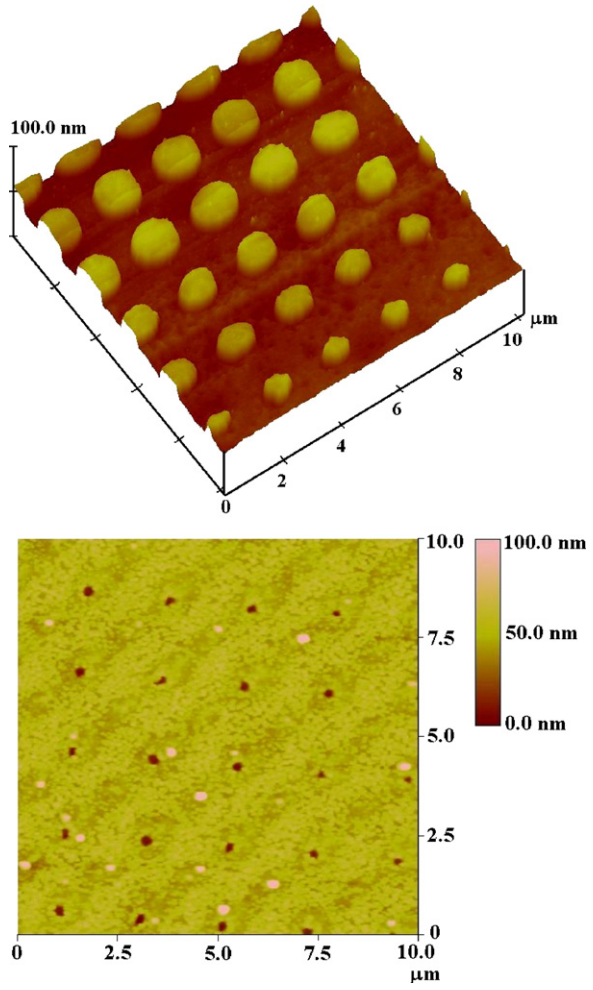

Fig. 8. AFM images of $Ge_1Sb_2Te_4$ and Sb_2Te_3 film (30 nm thickness) patterned by laser irradiation and then etched by 30% NaOH solution.

solution. The film thickness was 30 nm and patterned by laser irradiation. The $Ge_1Sb_2Te_4$ film was patterned by different fs laser pulse numbers, so the feature sizes were different. After dipping into NaOH solution, the amorphous surrounding was resolved. The height of each feature is 30 nm, which is exactly equal to the film thickness. The reaction velocity of crystalline features to NaOH solution was much slower than amorphous phase, which resulted in the formation of dots in pillar shape. Completely opposite reaction was found for Sb_2Te_3 film. It was crystalline features that were resolved for Sb_2Te_3 film, so the holes were left on the film.

It is found that other alkaline solution, such as KOH, has a similar etching function on phase change film. Fig. 9 is the dependence of crystalline feature height in $Ge_1Sb_2Te_4$ film on the etching time. The film thickness was 100 nm, and the etching solution was 30% KOH solution. It appears that at first 40 s, the etching rate is very slow. But the slope become steeper suddenly after 40 s, suggesting the etching rate increases faster from 40 s to 120 s. After 120 s, the etching rate becomes slower again and the amorphous phase is resolved completely, which means that it needs at least 2.5 min to resolve 100 nm phase change film in amorphous state.

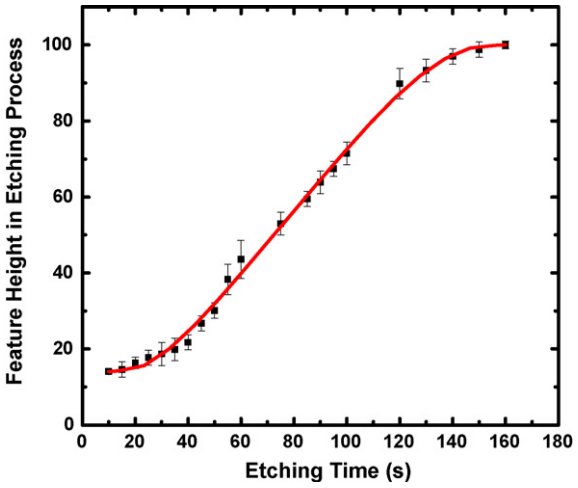

Fig. 9. Dependence of height of crystalline feature in 100 nm $Ge_1Sb_2Te_4$ film during etching process on the etching time, and the etching solution was 30% KOH solution.

The etching condition for Sb_2Te_3 film is quite different. The experiments suggest that the crystalline feature of Sb_2Te_3 film is etched very quickly. The crystalline features with depth of 100 nm can be etched away in less than 30 s. For longer time dipped into alkaline solution, the roughness of the film increased greatly, and the depth of the holes (left after crystalline features are resolved) decreased. It suggests that not only crystalline state of Sb_2Te_3 film is solved by the NaOH solution, but the amorphous phase also reacts to it though the reaction rate is slower. Such great difference of reaction rate of amorphous and crystalline phase states of $Ge_1Sb_2Te_4$ film and Sb_2Te_3 film to NaOH solution can lead to one conclusion that the Ge component plays important function for the chemical etching selectivity and rate. It seems that Ge drops the reaction rate of the phase change film to alkaline solution. Making use of this chemical etching method, three-dimensional rather than two-dimensional structures in the phase change film can be produced.

4. Conclusions

In this paper, laser micro/nanopatterning through MLA is demonstrated. The optical microscopy, AFM, EFM, and NSOM are used to characterize the topography, electrical and optical properties of phase change film. It suggests that the crystalline features have a higher reflectivity, while a lower transmitivity and resistivity than amorphous phase state. The characterization of features shows that the feature size increases with laser fluence linearly. The patterned phase change films are found to be active to the alkaline solution. The reactions of $Ge_1Sb_2Te_4$ and Sb_2Te_3 film to alkaline solution are quite different. In $Ge_1Sb_2Te_4$ film, the crystalline phase is inert to alkaline solution while the amorphous one is resolved easily. The Sb_2Te_3 film has not only completely opposite etching selectivity, but it is more active to alkaline solution as well. The reaction rate of two phase states of $Ge_1Sb_2Te_4$ film is much smaller than the Sb_2Te_3 film. It seems that Ge component in phase change film is most inert to the alkaline solution. In this way, 2D and 3D structures can be produced.

References

[1] A.N. Broers, J.M. Harper, W.W. Molzen, 250-Å linewidths with PMMA electron resist, Appl. Phys. Lett. 33 (1978) 392–394.
[2] D. Flanders, Replication of 175-Å lines and spaces in polymethylmethacrylate using X-ray lithography, Appl. Phys. Lett. 36 (1980) 93–96.
[3] M.A. McCord, R.F.P. Pease, Lithography with the scanning tunneling microscope, J. Vac. Sci. Technol. B 4 (1986) 86–88.
[4] T.R. Albrecht, M.M. Dovek, C.A. Lang, P. Grüter, C.F. Quate, S.W.J. Kuan, C.W. Frank, R.F.P. Pease, Imaging and modification of polymers by scanning tunneling and atomic force microscopy, J. Appl. Phys. 64 (1988) 1178–1184.
[5] K. Early, M.L. Schattenburg, H.I. Smith, Absence of resolution degradation in X-ray lithography for λ from 4.5 nm to 0.83 nm, Microelectron. Eng. 11 (1990) 317–321.
[6] J.W. Lyding, T.C. Shen, J.S. Hubacek, J.R. Tucker, G.C. Abelin, Nanoscale patterning and oxidation of H-passivated Si(1 0 0)-2 × 1 surfaces with an ultrahigh vacuum scanning tunneling microscope, Appl. Phys. Lett. 64 (1994) 2010–2012.
[7] S.Y. Chou, P.R. Krauss, P.J. Renstrom, Imprint of sub-25 nm vias and trenches in polymers, Appl. Phys. Lett. 67 (1995) 3114–3116.
[8] M.H. Wu, K.E. Paul, G.M. Whitesides, Patterning flood illumination with microlens arrays, Appl. Opt. 41 (2002) 2575–2585.
[9] J. Kato, N. Takeyasu, Y. Adachi, H.B. Sun, S. Kawata, Multiple-spot parallel processing for laser micronanofabrication, Appl. Phys. Lett. 86 (2005) 044102.
[10] H.F. Talbot, Phil. Mag. 9 (1836) 401–407.
[11] B. Besold, N. Lindlein, Practical limitations of talbot imaging with microlens arrays, Pure Appl. Opt. 6 (1997) 691–698.
[12] Y. Lin, M.H. Hong, G.X. Chen, C.S. Lim, Z.B. Wang, L.S. Tan, L.P. Shi, T.C. Chong, Microlens array patterning on phase change film, in: Proceedings of the 1st International Symposium on Functional Materials 2005, Kuala Lumpur, Malaysia, 2005, pp. 737–746.
[13] J. Kasparian, R. Sauerbery, D. Mondelain, S. Niedermeier, J. Yu, J.-P. Wolf, Y.-B. André, M. Franco, B. Prade, S. Tzortzakis, A. Mysyrowicz, M. Rodriguez, H. Wille, L. Wöste, Infrared extension of the super continuum generated by femtosecond terawatt laser pulses propagating in the atmosphere, Opt. Lett. 25 (2000) 1397–1399.
[14] N. Aközbek, A. Iwasaki, A. Becker, M. Scalora, S.L. Chin, C.M. Bowden, Third-harmonic generation and self-channeling in air using high-power femtosecond laser pulses, Phys. Rev. Lett. 89 (2002) 143901.
[15] H. Yang, J. Zhang, L.Z. Zhao, Y.J. Li, H. Teng, Y.T. Li, Z.H. Wang, Z.L. Chen, Z.Y. Wei, J.X. Ma, W. Yu, Z.M. Sheng, Third-order harmonic generation by self-guided femtosecond pulses in air, Phys. Rev. E 67 (2003) 015401.
[16] Z.Q. Hao, J. Zhang, Z. Zhang, T.T. Xi, Z.Y. Zheng, X.H. Yuan, Z.H. Wang, Third harmonic generation in plasma channels in air induced by intense femtosecond laser pulses, Acta Phys. Sin. 54 (2005) 3173–3177.
[17] H. Schillinger, R. Sauerbrey, Electrical conductivity of long plasma channels in air generated by self-guided femtosecond laser pulses, Appl. Phys. B 68 (1999) 753–756.
[18] S. Tzortzakis, M.A. Franco, Y.-B. André, A. Chiron, B. Lamouroux, B.S. Prade, A. Mysyrowicz, Formation of a conducting channel in air by self-guided femtosecond laser pulses, Phys. Rev. E 60 (1999) R3505–R3507.
[19] Y. Lin, M.H. Hong, W.J. Wang, Y.Z. Law, T.C. Chong, Sub-30 nm lithography with near-field scanning optical microscope, Appl. Phys. A 80 (2005) 461–465.
[20] Y. Lin, M.H. Hong, C.S. Lim, G.X. Chen, L.S. Tan, Z.B. Wang, L.P. Shi, T.C. Chong, Ultrafast laser induced parallel phase change nanolithography, Appl. Phys. Lett. 89 (2006) 041108.
[21] R. Waser, Nanoelectronics and Information Technology: Advanced Electronic Materials and Novel Devices, Wiley-VCH, Cambridge, Weinheim, 2002.
[22] N. Yamada, E. Ohno, K. Nishiuchi, N. Akahira, Rapid-phase transitions of GeTe-Sb_2Te_3 pseudobinary amorphous thin films for an optical disk memory, J. Appl. Phys. 69 (1991) 2849–2855.